Dimensional analysis and CFD simulations of microcarrier 'just-suspended' state in mesenchymal stromal cells bioreactors

Angélique Delafosse, Céline Loubière, Emmanuel Guedon, I. Chevalot, Dominique Toye, Eric Olmos

To cite this version:

Angélique Delafosse, Céline Loubière, Emmanuel Guedon, I. Chevalot, Dominique Toye, et al.. Dimensional analysis and CFD simulations of microcarrier 'just-suspended' state in mesenchymal stromal cells bioreactors. Chemical Engineering Science, 2019, 203, pp.464-474. 10.1016/j.ces.2019.04.001. hal-02151663

HAL Id: hal-02151663
https://hal.science/hal-02151663v1

Submitted on 22 Oct 2021

Dimensional analysis and CFD simulations of microcarrier 'just-suspended' state in Mesenchymal Stromal Cells bioreactors

C. Loubière[a], A. Delafosse[b,c], E. Guedon[a], I. Chevalot[a], D. Toye[b,c], E. Olmos[a,*]

[a] *Laboratoire Réactions et Génie des Procédés, Université de Lorraine, CNRS, LRGP, F-54000 Nancy, France*
[b] *Laboratory of Chemical Engineering, Université de Liège, Allée de la Chimie 3, B6C, 4000 Liège, Belgium*
[c] *Fonds de la Recherche Scientifique (FRS-FNRS), Rue d'Egémont 5, 1000 Bruxelles, Belgium*

Abstract

Large-scale Mesenchymal stem / stromal cells culture uses 3D culture systems involving spherical solid particles, called microcarriers. Cells adhere on these spheres, which are then set in suspension in stirred tank bioreactors. This work was more particularly focused on the determination of the critical impeller agitation rate N_{js}, allowing complete beads suspension. It is indeed generally assumed that this value is a good compromise between sufficient nutrients homogenization, mass transfer and minimization of hydromechanical stress encountered by the cells. However, no robust correlation predicting N_{js} in the case of microcarriers can be found in literature. To fill this lack, a set of various operating conditions was carried out, dealing with geometrical variables and two different microcarriers, and N_{js} were experimentally de-

---

[*] Corresponding author
Email address: `eric.olmos@univ-lorraine.fr` (E. Olmos)

Preprint submitted to Chemical Engineering Science *March 12, 2019*

termined for 140 conditions. An empirical correlation was established and a dimensional analysis was performed, showing that the impact of the particle concentration on N_{js} was function of the impeller design. Moreover, two dimensionless numbers characterizing the number of particle and an Archimede number applied on the particle cloud were found to better describe the impact of particle diameter and density on N_{js}. Simultaneously, a strategy based on Computational Fluid Dynamics simulations was conducted in order to predict N_{js} and was validated with the N_{js} experimental values.

Keywords: microcarrier suspension, bioreactor, critical just-suspended agitation rate, Computational Fluid Dynamics (CFD), dimensional analysis

1. Introduction

Today, still growing attention is paid to mesenchymal stem / stromal cell (MSC) culture for applications in regenerative medicine, with 843 MSC-based clinical completed or ongoing trials identified (www.clinicaltrials.gov, May 2018). Nevertheless, these cells are present in limited quantities in the human body, and this number decreases with the age of the donor [1]. An *ex-vivo* expansion phase is thus necessary to get sufficient cells quantities to meet the medical needs which are generally estimated between 10^9 and 10^{12} cells/lot [2]. As some other cell sources, MSCs are anchorage-dependent, namely they need to adhere on a surface to proliferate. Thus, MSCs are typically cultivated in static mode in 2D monolayer systems such as planar culture flasks. However, these devices hold some significant disadvantages for expansion process scale-up such as the storage of numerous flasks in incubators, the difficulty of operating conditions control, as well as the operational costs and the contamination risks.

To overcome these limits, cultures are now transposed on microcarriers, consisting of spheres of about 200 μm diameter with a density close to water one [3]. Once cells adhere on the surface of these particles, they are suspended in a bioreactor filled with the culture medium by mechanical agitation. The specific adherence surface available for cell expansion is greatly enhanced in comparison with 2D static culture, and the addition of monitoring / control loop is made easier, in accordance with GMP specifications. Moreover, mixing allows a better culture homogenization, limiting O_2, pH and nutrients gradients, enhancing mass transfer and available liquid-solid interfacial area maximization. It has been demonstrated that growth on microcarriers allows a higher number of cells recovered by lot, despite requiring more efforts and investments in R&D for a company currently using T-flasks to change to microcarrier based cultures [4, 5]. Recently, microcarrier MSC cultures have been successfully conducted at a few liter-scale [6, 7].

However, while a too low agitation would lead to microcarriers settling in the bottom of the vessel and aggregation [8], a too high agitation may generate damages to the cells [9], induce their differentiation [10] or lead to a failure of the cells to attach efficiently to the particles [11]. These damages may result from three separate mechanisms [12]: collisions with other microcarriers, collisions with bioreactor internals (wall, probes, other immersed equipment, and particularly the impeller) and interactions with turbulent eddies whose sizes are close to microcarriers one [13]. In that case, these authors showed that turbulent eddies led to direct shear damages on the microcarriers either by making them rotate at the Kolmogorov velocity scale, or entrap them in counter-rotating eddies. One reasonable strategy to get a sufficient mixing performance and minimization of hydromechanical stress is to operate at the impeller just-suspended agitation rate N_{js} allowing complete bead suspension. This means that bioreactor hydrodynamics have to be therefore intensively studied to guarantee cells viability and allow a process scale-up [14], requiring reliable model and numerical tools. Many methods were established to estimate N_{js}, and some of them were well-developed in [15]. They were classified in 3 categories: (i) 'empirical methods' with direct methods like the Zwietering visual method [16, 17, 18] stating that when N_{js} is reached, particles do not stay longer than 1 or 2 seconds in the vessel bottom, and indirect methods like the cloud height method [19], the particle concentration determination using light attenuation technique [20] or the power number method [21], (ii) 'numerical methods' based on data recovered from CFD simulations [22, 23], and (iii) finally 'theoretical methods'. In the last case, investigations were mainly based on the assumption of an equilibrium between particle settling and the off-bottom lifting [24, 25, 26] and led to models derived from experimental results, according to limited ranges of geometries and particle properties. The most commonly used was developed by Zwietering [16] and is presented in Eq. (1).

$$N_{js} = S \cdot \nu_L^{0.1} \cdot \left(\frac{g.(\rho_p - \rho_L)}{\rho_L} \right)^{0.45} \cdot X^{\,0.13} \cdot d_p^{0.2} \cdot D^{\,-0.85} \tag{1}$$

Where X is the particle mass fraction and S is a dimensionless parameter related to the geometry of the vessel and the impeller, via the ratio of the impeller diameter on the tank diameter D/T, the ratio of the off-bottom clearance on the tank diameter C/T and the impeller design. With these dimensionless parameters, S is independent of the scale of the system but not of the system geometry. However, this correlation was established and validated for particles that were significantly denser than microcarriers, like sand or glass beads. It was shown by [27] that the calculation of the S coefficients using Eq. (1), in the same operational conditions, could present up to 50 % overestimation for microcarriers. This difference was attributed to the low density difference between the solid and the liquid phases (around 40 kg m^{-3}) in the case of microcarriers, which facilitates the lifting of particles from the tank bottom.

Complementary studies were conducted on the determination of N_{js} and its dependence on geometrical, physical and operational variables like, among others, the effects of the low off-bottom impeller clearance or the bottom shape on flow patterns evolution [28, 29], the impacts of the solid volume fraction incorporated in the reactor [30], or in the specific case of microcarriers, the type of microcarriers used [31] and the impeller design leading to different possible agitation modes [32]. Recently, microcarrier suspension were also characterized in orbital shakers and led to the establishment of a new correlation predicting N_{js}. A dimensional analysis provided the most appropriate geometrical characteristics for cell cultures [33]. However, despite all of these efforts, no robust correlation predicting N_{js} can be found in the literature for microcarrier suspension in stirred tank bioreactors.

To fill this lack, the present study was focused on the numerical prediction of N_{js} in the specific case of microcarriers. To do that, the critical agitation rate N_{js} was experimentally determined for 140 operating conditions in the case of a hemispherical-bottom shape bioreactor. A dimensionless equation was then established using these data. Simultaneously, a strategy based on Computational Fluid Dynamics (CFD) simulations was conducted in order to predict N_{js} for specific operating conditions of the cell culture. In this study, the CFD simulations of particles suspension were validated using the collected experimental data. As a complementary approach to experiments, these preliminary CFD simulations were more particularly motivated by mid-term perspectives of numerical applications, such as (*i*) study of the impact of culture system on the spatial distribution of the particles, (*ii*) the simulation of particle 'lifelines' within the bioreactor and particle-particle interactions or (*iii*) the definition of *a priori* scale-up rules.

2. Experimental approach

2.1. Design of experiment

The bioreactor investigated was a hemispherical-bottom transparent glass vessel equipped with three probes (dissolved oxygen, pH and temperature) on the head plate. It was filled with Dulbecco's Phosphate Buffered Saline solution (DPBS) for a working volume of 1.12 L, at which the liquid height corresponded to the vessel diameter $H = T = 0.12$ m. The temperature was controlled and regulated at 20°C, at which the liquid properties were considered to be the same as water, and a baffle was added to the pH probe in order to avoid vortex formation during the agitation. Operating conditions were chosen to cover a wide range of values for five parameters related to microcarriers, impeller, and design characteristics (Fig. 1 ; see supplementary material 1).

Firstly, the impeller geometry impact was investigated by changing the

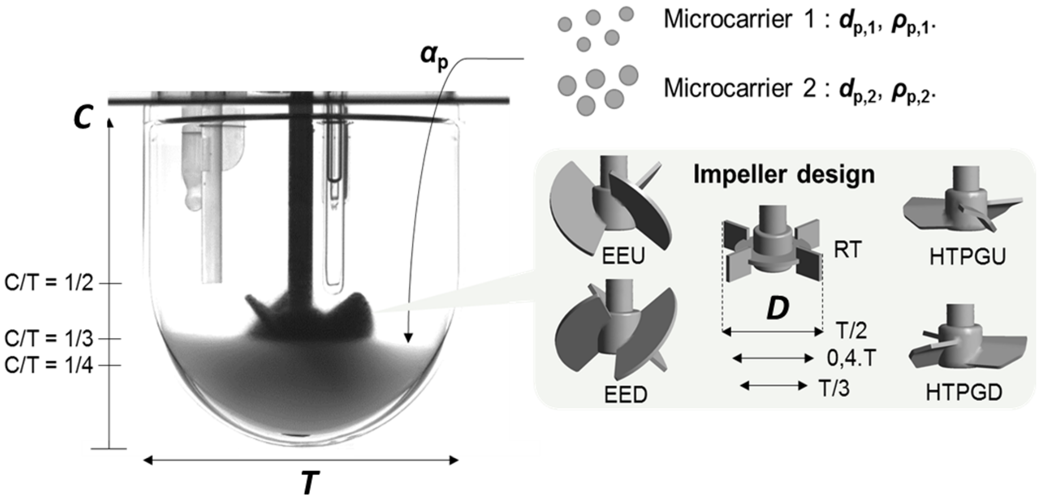

Figure 1: Variables used to define the operating conditions: the off-bottom clearance C and the impeller diameter D in function of the tank diameter T, the type of microcarrier with their specific diameters and density, the particle volume fraction α_p, and the impeller design with the Ear Elephant in up-pumping (EEU) and down-pumping (EED) modes, the HTPG impeller up-pumping (HTPGU) and down-pumping (HTPGD) and the Rushton turbine (RT).

impeller design and two geometrical ratios: D/T, defining the impeller diameter on the vessel diameter, and C/T, defining the off-bottom clearance on the vessel diameter ratio. More specifically, three impeller designs were studied: a radial four-blade Rushton Turbine (RT), an axial 3-blade impeller (HTPG) and an Elephant Ear impeller (EE). Both axial impellers were studied in up-pumping and down-pumping modes, allowing at least five agitation types. Each impeller was available at three D/T ratios: 0.33, 0.4 and 0.5, and placed according to three possible C/T ratios: 0.5, 0.33 and 0.25. In this study, the off-bottom clearance C was considered as the distance between the vessel bottom and the bottom side of the impeller hub.

Secondly, microcarrier properties impact on N_{js} was determined by varying the particle volume fraction α_S and the type of microcarrier used. Two different microcarriers were investigated: the Cytodex-1 (GE Healthcare) composed of a cross-linked dextran matrix with positively charged N, N-dietylaminoethyl groups, and the Star-Plus (Pall SoloHill) composed of a polystyrene core and featuring a surface chemistry with a net positive charge. Cytodex-1 microcarriers swell when put in solution. Their swelling factor, and thus their diameter and density, depend on the salt concentration of the solution. After spending a night in a phosphate buffer saline (DPBS) solution, the diameter distributions were established from microscope pictures and their density was estimated from their swelling factor and the density of the dry microcarriers (see [20] for details). The same procedure was also applied to Star-Plus microcarriers. The physical properties assumed for all the study were the experimental data given in Table 1. For comparison, the values provided by the manufacturer were also reported. Five microcarrier volume fractions ranging from 1 to 12 % were investigated, corresponding to the concentrations classically used during cell cultures.

Table 1: Microcarrier physical properties: manufacturer and experimental data.

	Manufacturer data			Experimental data			
Microcarrier	ρ_P kg m^{-3}	d_{50} µm	d_{5-95} µm	ρ_P kg m^{-3}	d_{50} µm	d_{5-95} µm	d_{mean} μm
Cytodex-1	1030	190	150-250	1018	170	140-200	180
Star-Plus	1020-1030	N/A	125-212	1020	150	120-170	160

2.2. Experimental suspension criterion and N_{js} visual determination

The vessel was placed in an aquarium with a mirror added below, permitting a better visualization and N_{js} was visually established by particle movements at the bottom of the vessel using the protocol of Zwietering criterion [20]. For each N_{js} determination, two measurements strategies were performed. For the first one, all particles were settled in the vessel bottom with no agitation followed by a slow increase of the agitation rate until just-suspended state $N_{js,\ up}$. For the second one, agitation rate was progressively reduced from complete suspension to just-suspended state $N_{js,\ down}$. For all operating conditions, it was noted that these two agitation rate values remained significantly closed from one to each other (mostly a difference of two RPM). Thus, $N_{js,\ up}$ will be used as N_{js} in the rest of the study to mimic the N_{js} investigation during cultures. 95 operating conditions were used for the model resolution. The model was then validated using 45 other operating conditions.

3. Particle suspension modelling

3.1. Zwietering correlation validity

First, the N_{js} experimentally collected were used to verify the Zwietering correlation given in Eq. 1, by calculating the experimental S coefficients which are a function of the impeller design, D/T and C/T ratios and the vessel bottom shape. It was also assumed that S is independent of other parameters, such as the solid volume fraction α_S or the particle physical properties ρ_p and d_p. Since not all S coefficients of the experimental conditions presented in the present study were available in the literature, particularly with a hemispherical vessel bottom shape, experimental S can not be directly compared to their theoretical values. However, if it was assumed that they are not dependent of the particle volume fraction and particles diameter and density, S should stay constant while only these parameters were varied. This was verified for two different microcarriers at particle volume fractions between 1 % and 12 %. If significant variations were observed between the different experimental values, it would deny the model proposed by Zwietering (Eq. 1) for microcarrier suspension.

3.2. Dimensional analysis

The targeted variable N_{js} was determined according to the 9 following physical parameters:

- Geometrical parameters including T the tank diameter, D the impeller diameter and C the off-bottom clearance.

- Material properties of the liquid phase (density ρ_L and dynamic viscosity μ_L) and of the solid phase (density ρ_p, diameter d_p and volume fraction α_S).

- Gravity acceleration g.

These parameters were considered independent and involved 3 fundamental dimensions, namely mass, length and time. According to the Vachy-Buckingham theorem, these 10 variables may be related by a relationship between 7 dimensionless numbers. The following dimensionless ratios π_i were thus constructed:

$$\pi_1 = \frac{N_{js} \cdot T^2 \cdot \rho_L}{\mu_L}, \quad \pi_2 = \frac{C}{T}, \quad \pi_3 = \frac{D}{T}, \quad \pi_4 = \frac{d_p}{T},$$

$$\pi_5 = \alpha_S, \quad \pi_6 = \frac{g \cdot T^3 \cdot \rho_L^2}{\mu_L^2}, \quad \pi_7 = \frac{\rho_p}{\rho_L}.$$

By looking for their physical meaning, they were adapted into the 6 following dimensionless ratios:

- Geometrical ratios: $\frac{C}{T}$, $\frac{D}{T}$ and $\frac{d_p}{D}$.
- Reynolds number: $\frac{\rho_L \cdot N_{js} \cdot D^2}{\mu_L}$.
- Solid volume fraction: α_S.
- Liquid viscosity ratio $\mu^* = \frac{\mu_L}{(\rho_p - \rho_L) \cdot g^{0.5} \cdot T^{1.5}}$.

The last parameter μ^* was adapted from Olmos *et al.* [33], obtained from the dimensional analysis established for microcarrier suspension in orbital shaken bioreactors. A second set of dimensionless parameters was proposed with the following ratios:

- Geometrical ratios: $\frac{C}{T}$ and $\frac{D}{T}$.
- Reynolds number: $\frac{\rho_L \cdot N_{js} \cdot D^2}{\mu_L}$.
- Solid volume fraction: α_S.
- Archimede number of the particle cloud: $\frac{g \cdot \alpha_S \cdot T^3 \cdot \rho_L \cdot (\rho_p - \rho_L)}{\mu_L^2}$.
- Dimensionless number related to the particle number: $\left[\alpha_S \cdot \left(\frac{T}{d_p}\right)\right]^3$.

On the basis of the experimental data, three monomial models were build and the most robust N_{js} model was determined. The first one, given in Eq. (2) expressed N_{js} directly as a function of α_S, C, D and d_p, whereas the two others presented in Eqs. (3) and (4) involved the two set of dimensionless ratios, with the targeted variable N_{js} through the Reynolds number Re_{js}.

Model 1

$$N_{js} = K_1 \cdot \alpha_S^{a_1} \cdot C^{\,b_1} \cdot D^{\,c_1} \cdot d_p^{d_1} \tag{2}$$

Model 2

$$\begin{aligned} Re_{js} = K_2 \cdot \alpha_S^{a_2} \cdot \left(\frac{C}{T}\right)^{b_2} \cdot \left(\frac{D}{T}\right)^{c_2} \cdot \left(\frac{d_p}{D}\right)^{d_2} \\ \cdot \left(\frac{\mu_L}{(\rho_p - \rho_L) \cdot g^{0.5} \cdot T^{1.5}}\right)^{e_2} \end{aligned} \tag{3}$$

Model 3

$$\begin{aligned} Re_{js} = K_3 \cdot \alpha_S^{a_3} \cdot \left(\frac{C}{T}\right)^{b_3} \cdot \left(\frac{D}{T}\right)^{c_3} \cdot \left[\alpha_S \cdot \left(\frac{T}{d_p}\right)^{3}\right]^{d_3} \\ \cdot \left(\frac{g \cdot \alpha_S \cdot T^{\,3} \cdot \rho_L \cdot (\rho_p - \rho_L)}{\mu_L^2}\right)^{e_3} \end{aligned} \tag{4}$$

In Eqs. (2) - (4), K_i are constants characterizing the impeller design and a_i, b_i, c_i, d_i and e_i are the exponents to which the parameters or dimensionless numbers were raised to. It is important to emphasize that in this study d_p, ρ_p and the liquid properties, ρ_L and μ_L, were specific to microcarriers and chosen in the industrial context of animal cell culture. Hence, d_p and ρ_p belonged to a narrow range of values, with a density close to the liquid phase similar to water. The phase density difference was found very sensitive in the model resolution, caused by very low values and inaccuracies. So, $(\rho_p - \rho_L)$ was not included in the first model (Eq. (2)), and e_i exponents for model 2 and 3 (Eqs. (3) and (4)) were not possible to determine by experimental data fit. Consequently, another strategy was adopted to calculate these values. It was indeed demonstrated by Mersmann *et al.* that particle suspensions occurred at constant (P/V) ratios for systems with geometrical similarities [24]. The model proposed should thus respect this assumption to be consistent, so e_i coefficients were calculated in order to keep constant the $(P/V)_{js}$ ratio defined in Eq. (5).

$$\left(\frac{P}{V}\right)_{js} = \frac{N_p(N = N_{js}) \cdot \rho_L \cdot N_{js}^3 \cdot D^5}{V} \tag{5}$$

In the present study, Reynolds numbers were calculated between 1000 and 12000. Without reliable N_p measurements in a such small volume, N_p was nevertheless considered steady in this flow regime. A constant $(P/V)_{js}$ would lead to the equation (6).

$$\frac{N_{js}^3 \cdot D^5}{T^3} \propto 1 \tag{6}$$

In order to reduce the number of exponents to be solved, (D/T) exponent determination was based on the literature. In one hand, the Zwietering model (Eq. (1)) proposed a value of -0.85, admitting that the model constant was also function of the impeller diameter. In the other hand, Nienow *et al.* extracted the impeller variable from the constant and obtained a final exponent of -2.21 [17]. The present models were thus solved for different values comprised between these two bounds. They were solved by using an optimization algorithm (non-linear, GRC, Excel, Microsoft) in order to get the last exponent values a_i, b_i and d_i. The objective of this optimization consisted in minimizing the criterion $\omega = \sum_{i=0}^{n_{exp}} (N_{js}^{mod} - N_{js}^{exp})^2$ with N_{js}^{mod} and N_{js}^{exp} were respectively the modeled and the experimental values of N_{js}. Models were finally validated for 40 operating conditions chosen out of the previous set of operating conditions defined for the the model solving, and involving different impellers at different particle volume fractions between 1 and 19 %. An additional N_{js} data (Cytodex-1 at a volume fraction of 18.5 %) was recovered from the literature for the case of an Elephant Ear impeller ($D/T = 1/2$ and $C/T = 1/3$) in down-pumping mode placed in a 20 L hemispherical bioreactor, geometrically similar to the one used in the present study [34]. Models were applied for these operating conditions to verify their scalability. A last validation at the temperature of 37°C, generally used in cell culture, was performed by comparing experimental N_{js} values to the predicted ones at 20 and 37°C and for 4 different impellers.

3.3. Multiphase simulation by CFD

3.3.1. CFD simulations

CFD simulations were performed by using the commercial finite volume solver ANSYS Fluent (ANSYS Inc., version 16.1). A granular Euler-Euler RANS (Reynolds Averaged Navier-Stokes) approach was applied, considering two interpenetrating phases. The continuity and momentum equations were solved for each phase in steady-state by using the Moving Reference Frame (MRF) approach to model the impeller rotation. The Reynolds stress tensor $\overline{\overline{\tau}}$ was modelled by the standard k-ε turbulence model, previously validated for particles at the just-suspended state [15] and for microcarrier suspensions [35, 36, 37], despite Reynolds numbers related to a transitional regime.

Among other set of models, Delafosse *et al.* demonstrated that this model led to the most robust results [20]. Two dominant fluid/solid interactions were considered with the drag and the turbulent dispersion forces. These two conservation equations were developed in Eqs. (7) and (8) for the liquid phase, and Eqs. (9) and (10) for the solid phase.

$$\begin{cases} \nabla \cdot (\alpha_L \rho_L \boldsymbol{v_L}) = \nabla(\gamma_L \nabla \alpha_L) & (7) \\ \nabla \cdot (\alpha_L \rho_L \boldsymbol{v_L v_L}) = -\alpha_L \nabla p + \nabla \cdot \overline{\overline{\tau}}_L \\ \qquad\qquad + \alpha_L \rho_L \boldsymbol{g} + K_{LS}(\boldsymbol{v_S} - \boldsymbol{v_L}) & (8) \end{cases}$$

$$\begin{cases} \nabla \cdot (\alpha_S \rho_S \boldsymbol{v_S}) = \nabla(\gamma_S \nabla \alpha_S) & (9) \\ \nabla \cdot (\alpha_S \rho_S \boldsymbol{v_S v_S}) = -\alpha_S \nabla p - \nabla p_S + \nabla \cdot \overline{\overline{\tau}}_S \\ \qquad\qquad + \alpha_S \rho_S \boldsymbol{g} + K_{LS}(\boldsymbol{v_L} - \boldsymbol{v_S}) & (10) \end{cases}$$

Where $\boldsymbol{v}$ was the velocity of the corresponding phase, p the pressure shared by all phases and $\boldsymbol{g}$ the acceleration due to gravity. The interphase drag force involved the interphase momentum exchange coefficient K_{LS}, modelled by the Huilin-Gidaspow equations (ANSYS Fluent theory guide [38]). The diffusion-in-VOF equation was used to model the turbulent dispersion and was included in the mass conservation equation through $\nabla(\gamma_L \nabla \alpha_L)$ and $\nabla(\gamma_S \nabla \alpha_S)$ terms.

Cytodex-1 particles were chosen as reference particles for the simulations, defined by the experimental mean diameter and density. Based on experimental observations of bed height, the value of the packing limit was estimated to 0.6, which was a value close to the solid fraction of randomly packed spheres of equal diameter (0.63). However, the impact of the value of the packing limit was negligible in our simulations as the maximal volume fractions obtained remained lower than 0.3 approximately. It should be noticed that microcarriers are also non-porous particles. Calculation domain was discretized using between 230000 and 275000 tetrahedral meshes of around 5 mm, except in a zone in the vessel bottom, where the size was refined at a maximum of 2 mm, as presented in Fig. 2 to allow a better description of particle just-suspended state. This number of mesh cells was chosen as a compromise between a reasonable calculation time and a sufficient accuracy for the results analysis. To validate the choice of the $\approx$ 250k cells grid, calculations were also performed for two cases using a finer grid of $\approx$ 1M cells. First one (A) was impeller EED with C/T = 0.5 ; D/T = 0.4 and alpha = 12 % and second one (B) was impeller HTPGD, C/T = 0.5, D/T = 0.5, alpha = 4 %. While errors between experimental Njs measurements and 250k grid calculations were respectively of 1.5 and 2.6 % for cases A and B, it reached respectively 14.7 and 7.8 % with the 1M cells grid. Thus, the 250k cells grid was finally used for the complete set of simulations.

The simulation was initialized, considering all particles quasi-settled ($\alpha_S =$ 0.5) at the bottom of the bioreactor. Higher particle concentrations led to divergence during the first iterations. Consequently, 0.5 was found to be a good compromise, allowing particles settling during the first iterations and avoiding divergence. Convergence of the simulations was supposed when equation residuals were less than 10^{-5} and when liquid velocities and solid volume fractions in the impeller vicinity were stabilized. This second validation was necessary to ensure the stabilization of the N_{js} determination

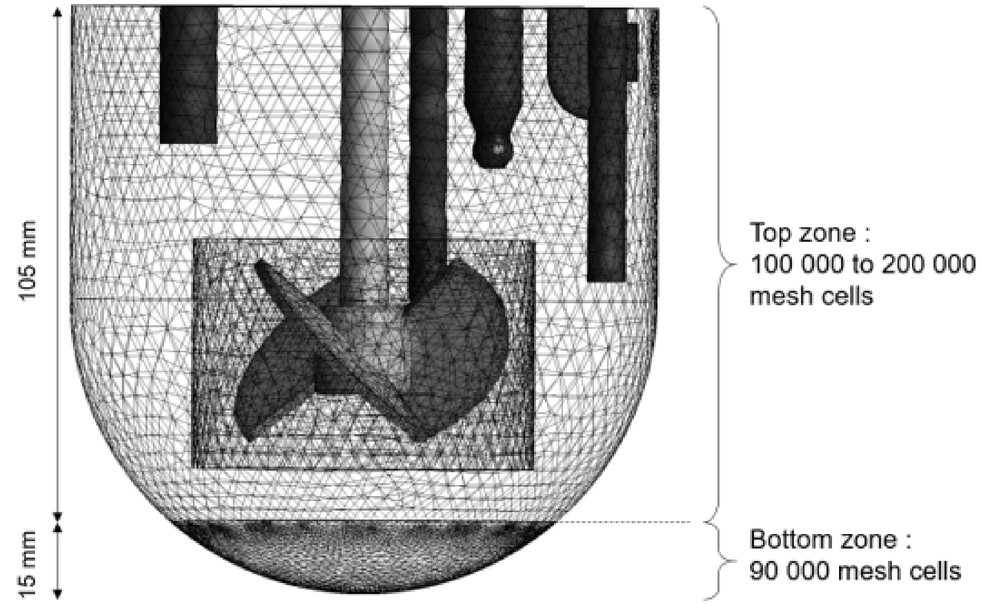

Figure 2: Mesh discretization of the vessel for the CFD simulations.

criterion presented in the next following part.

3.3.2. N_{js} determination strategy by using CFD

To model the subjective experimental determination of N_{js}, two simulation outputs were proposed.

The first one Packed Fraction PF related the volume of packed particles to the total volume of particles. To determine the value of PF, particles were supposed packed if their local volume fraction was between $\alpha_{ref} = 0.55$ and the packing limit 0.6 (Eq. 11).

$$PF = \frac{V_p\ (\alpha_p > \alpha_{ref})}{V_{p,\,tot}} \tag{11}$$

The second one, Still Fraction SF (Eq. 12), related the volume of 'quasi-motionless' particles on the total volume of particles. It was based on the determination of the local particle residence time τ_p in mesh cells in the bottom of the system. If this value was smaller than a reference residence time based on a time of 1 second to pass through a cube with 2 mm sides, then particles were considered to be almost motionless in the mesh cell. Experimentally, last microcarriers to be lifted tended to stay closely together by forming a little cone with a slow circular movement. SF reflected this phenomenon and returns the percentage of particles in this situation.

$$SF = \frac{V_P\ (\tau_p < \tau_{ref})}{V_{p,\ tot}} \tag{12}$$

As considered by Tamburini *et al.* [22] with the development of their CFD method *Unsuspended Solids Criterion*, the results were dependent of the grid and the volume discretization. A coarse grid could lead to uncertainties and to underestimations of N_{js} values. In the present study, the finer meshing in the bottom zone permitted to limit this effect.

Using these two criteria, a CFD-based strategy was developed to reach the value of N_{js} by a progressive decrease of the agitation rate N until a predefined critical value of PF or SF was reached. Preliminary simulations were performed in a 200 mL minibioreactor with the experimental data recovered from Collignon *et al.* works [32]. The strategy consisted in preliminary validation in a scale-down geometry. Hence, this step allowed to valid the chosen models and to define the critical values of the two parameters defining the just-suspended state of particles: $PF^{\,crit}$ and $SF^{\,crit}$. After this first validation, the method was transferred to the geometry of the 1.12 L reactor of this study. The approach was validated for various geometrical conditions and particle concentrations in the case of the HTPG and the Ear Elephant impellers in down-pumping mode. Then, the method was applied at one or two operating conditions of the Rushton turbine and the HTPG and Ear Elephant impellers in up-pumping mode.

4. Results and discussions

4.1. Suspension modelling

First, S coefficients of the Zwietering correlation presented in Eq. (1) were calculated from 8 experimental N_{js} measurements, by reorganizing Eq. (1) into Eq. (13). They all shared the same impeller conditions: an HTPG impeller in down-pumping mode, at a D/T ratio of 0.5 and a C/T ratio of 0.5. These S values are presented in function of the microcarrier volume fraction α_S in Fig. 3. On the contrary to what was commonly admitted, it can be noted that, in the case of microcarriers, S depended on the value of α_S with a 27 % deviation between the lowest and the highest values of S. Thus, exponents of the Zwietering correlation should be revisited, especially concerning the terms involving the microcarrier properties.

$$S = \frac{N_{js}}{\nu_L^{0.1} \cdot \left(\frac{g.(\rho_p - \rho_L)}{\rho_L}\right)^{0.45} \cdot X^{\,0.13} \cdot d_p^{0.2} \cdot D^{\,-0.85}} \tag{13}$$

The five impellers could be classified in three types, according to the flow patterns induced and microcarrier bed shapes. With increasing agitation rates, the bed progressively evolved from a planar-surface volume to a cone shape for both radial flow (RT) and mixed-flow (EEU and HTPGU)

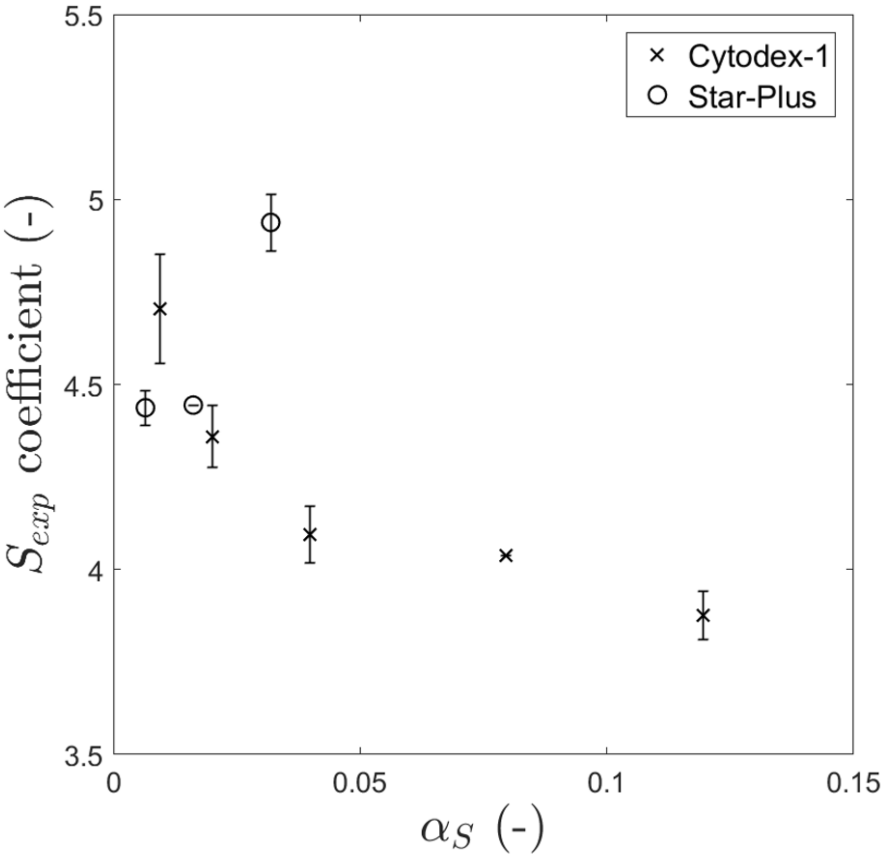

Figure 3: Evolution of the experimentally determined S coefficient from the Zwietering correlation with the microcarrier volume fraction in the bioreactor, for Cytodex-1 and Star-Plus.

impellers, as presented in Fig. 4 (B and C). Particles were pushed inward and driven by the impeller. With axial flow (EED and HTPGD) the bed was a peakless cone as shown in Fig. 4 (A). In this case, particles were pushed down and suspended after sliding along the side wall. Thus, these three flow patterns involved different suspensions phenomena, which were taken into account for the model establishment. The consequence on parameter fitting

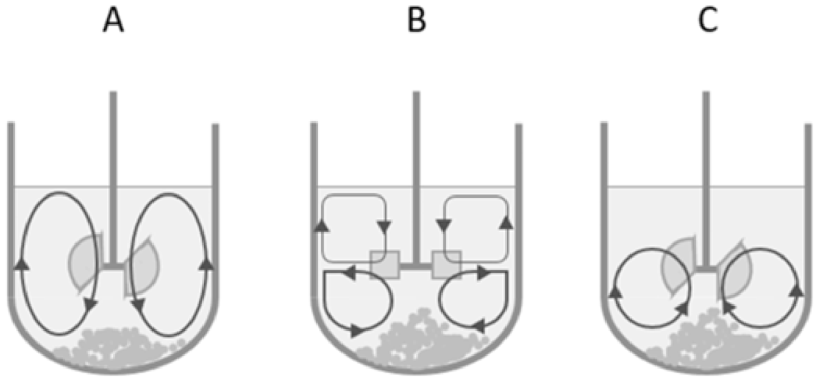

Figure 4: Flow patterns and particles bed shapes observed at agitation rates $N < N_{js}$ depending on mixing structures: axial flow with EED and HTPGD (A), radial flow with RT (B) and mixed-flow with EEU and HTPGU (C).

was that, despite it could be possible to determine a unique set of parameters b_i, c_i and d_i for the three flow patterns, the exponents related to particle volume fraction had to be specific to each of them. The model constants K_i logically depended on impeller geometry. Best fitted models are given in Eqs. (14) - (16) and the parameters K_i given in Table 2, were only dependent on the impeller design. The coefficients a_1, a_2 and a_3 displayed three values according to the flow pattern and are given in table 2. a_1 and a_2 were the only exponents involving α_S. Considering Model 3 (Eq. (16)), α_S was involved in three terms, with $\alpha_S^{0.3}$, $\alpha_S^{0.4/3}$ and $\alpha_S^{14/45}$, consequently, a total exponent $Tot.\ \alpha_S\ exponent$ was calculated as $Tot.\ \alpha_S\ exponent = a_3 + 0.4/3 + 14/45$.

Model 1

$$N_{js} = K_1 \cdot \alpha_S^{a_1} \cdot C^{1/3} \cdot D^{-1} \cdot d_p^{-0.4} \tag{14}$$

Model 2

$$Re_{js} = K_2 \cdot \alpha_S^{a_2} \cdot \left(\frac{C}{T}\right)^{1/3} \cdot \left(\frac{D}{T}\right)^{0.6} \cdot \left(\frac{d_p}{D}\right)^{-0.4} \cdot \left(\frac{\mu_L}{(\rho_p - \rho_L) \cdot g^{0.5} \cdot T^{1.5}}\right)^{-28/75} \tag{15}$$

Model 3

$$Re_{js} = K_3 \cdot \alpha_S^{a_3} \cdot \left(\frac{C}{T}\right)^{1/3} \cdot \left(\frac{D}{T}\right)^{1} \cdot \left[\alpha_S \cdot \left(\frac{T}{d_p}\right)^{3}\right]^{0.4/3} \cdot \left(\frac{g \cdot \alpha_S \cdot T^{3} \cdot \rho_L \cdot (\rho_p - \rho_L)}{\mu_L^2}\right)^{14/45} \tag{16}$$

Table 2: K_i and a_i parameters of the three models predicting N_{js}, according to the impeller design.

Flow pattern	Impeller	K_1 ($\times 10^{-3}$)	K_2	K_3	a$_1$	a$_2$	a$_3$	*Tot.* α_S *exponent*
(A)	HTPGD	7.9	8.2	2.4	0.07	0.07	-0.37	0.07
(A)	EED	4.9	5.0	1.5	0.07	0.07	-0.37	0.07
(B)	RT	6.3	6.4	2.0	0.1	0.1	-0.34	0.1
(C)	HTPGU	6.7	6.8	2.0	0.2	0.2	-0.24	0.2
(C)	EEU	4.9	5.1	1.5	0.2	0.2	-0.24	0.2

These three models were applied on 40 operating configurations out of the operating conditions defined for the models solving. The experimental measurements were performed by three different operators to include the potential subjective N_{js} determination, and involved the HTPG impeller in down-pumping mode, the Elephant Ear impeller in up-pumping mode and the Rushton turbine at different C/T ratios and at different particle volume fractions. Results are presented in Fig. 5 for model 3. Models were globally validated but presented deviations for high particle volume fractions with the Elephant Ear impeller. The model establishment was based on data involving particle volume fractions up to 12 % and did not seem thus suitable for higher concentrations with this type of impeller. However, these high microcarrier volume fractions are seldom used in animal cell culture bioreactors. Considering the 95 configurations of the design of experiments and the 40 complementary measurements, mean relative errors under 10 % were obtained for the three models. Mean errors obtained with each model are presented for the different impeller designs in Table 3.

Table 3: Mean errors between N_{js} predicted by the models and experimental values at T = 20°C, according to the impeller design and the model used.

	Model		
	1	2	3
HTPGD	6.0 %	6.0 %	5.8 %
EED	8.6 %	8.4 %	8.6 %
RT	11.1 %	12.8 %	11.5 %
HTPGU	9.3 %	8.9 %	8.9 %
EEU	12.3 %	13.2 %	12.5 %
Mean error	8.7 %	9.1 %	8.7 %

In order to determine the most robust model between the three proposed, the validity of each model was verified at the cell culture working temperature of 37°C and for a scale-up application in a 20 L vessel. Concerning the

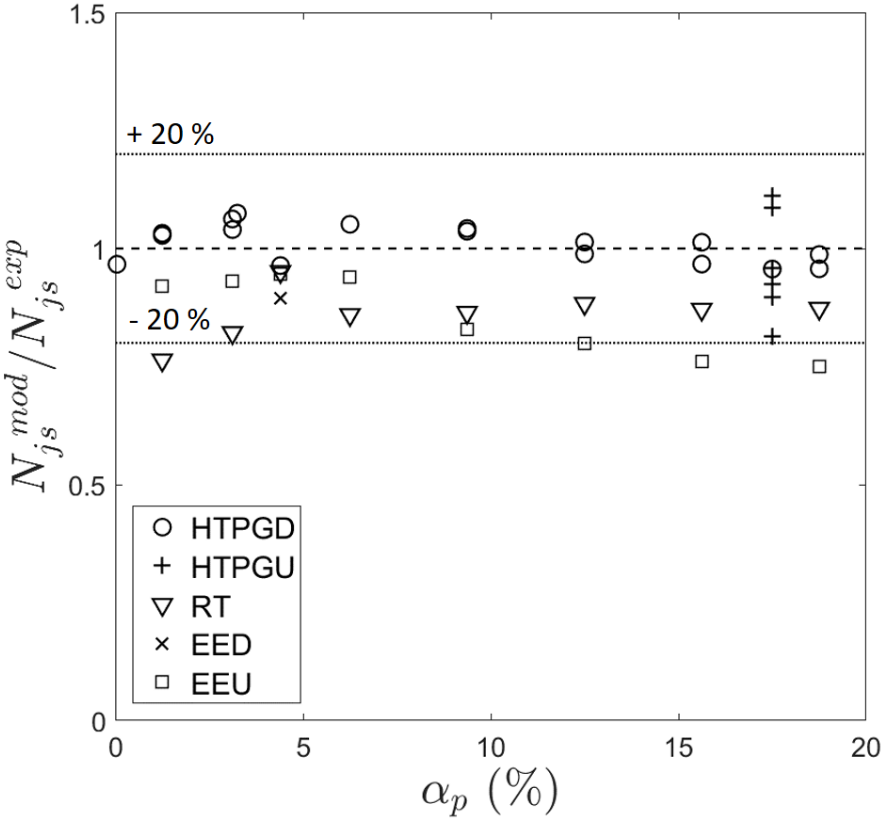

Figure 5: Comparison of the deviation between the experimental N_{js} and the N_{js} predicted by the model for operating conditions out of the design of experiment and model resolution.

temperature stability, fluid properties were admitted to be the same as water, with both density and viscosity dependent of the temperature. Results for four impeller designs are given in Table 4. All models presented mean deviations of less than 20 % between the experimental values and the predicted values, but model 2 (Eq. (15)) was found to be more robust than the others. Concerning the model scalability, results are presented in Table 5. In this case, the model 2 presented the highest deviation of 34 %. Consequently, model 1 (Eq. (14)) and model 3 (Eq. (16)) were found to be more suitable.

Regarding the mean relative error, the temperature validity, the scalability, and the physical meanings of each parameters, model 3 (Eq. (16)) was considered to be the best compromise. The comparison between the predicted values N_{js}^{mod} and the experimental values N_{js}^{exp} is reported in Fig. 6 for particle volume fractions under 12 %. A Student's t-test was performed with a statistical significance chosen at 0.05. Due to the distinct values of K_3 and a_3 coefficients according to the impeller design, t-tests were applied separately for each impeller design. For each of them, a regression analysis led to p-values of less than 0.01, indicating that all parameters of the model were statistically significant. This model will be used for the following discussion on the impact of each parameter, characterizing the operating conditions, on N_{js}. For the sake of clarity, K_3 and a_3 will be respectively renamed K and a.

Table 4: Mean errors between N_{js} predicted by the models and experimental values, at 37°C according to the impeller design and the model used.

	Model		
	1	2	3
HTPGD	18.5 %	0.5 %	15.1 %
EED	22.5 %	6.1 %	20 %
RT	15.1 %	7.2 %	11.3 %
EEU	19.1 %	0.9 %	15.3 %
Mean error	18.8 %	3.7 %	15.4 %

Table 5: Mean errors between N_{js} predicted by the models and experimental values at 20 rpm, in a 20 L vessel equipped with a EE down-pumping impeller, according to the impeller design and the model used.

Model	N_{js}^{mod} (rpm)	Deviation
1	21	5 %
2	27	34 %
3	22	11.2 %

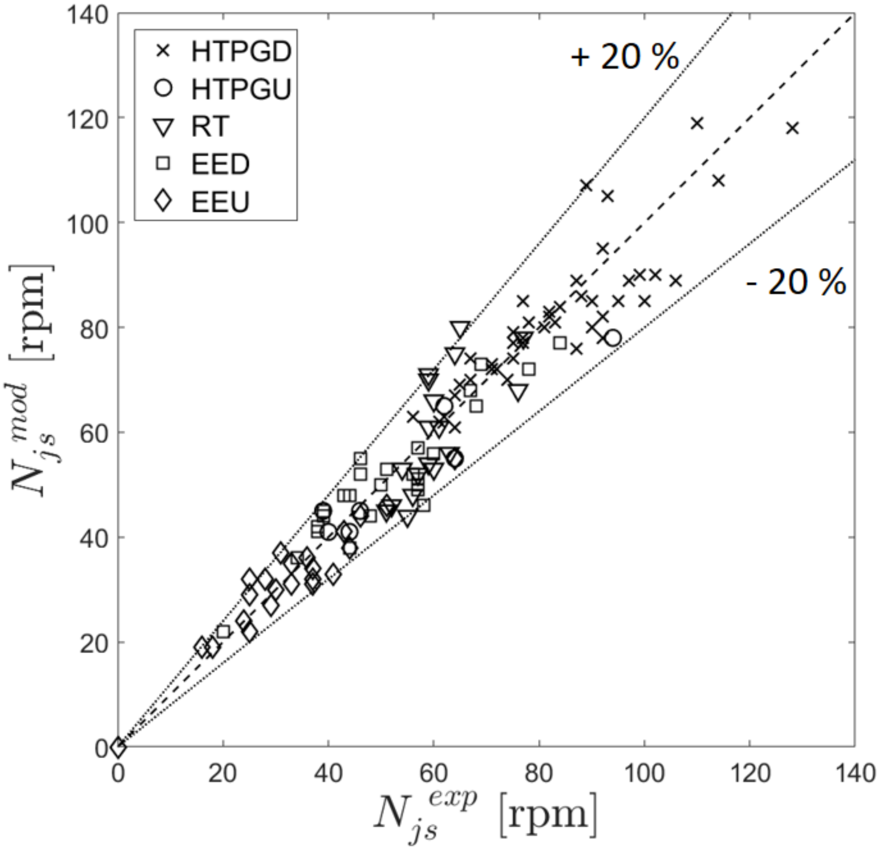

Figure 6: Comparison of experimental N_{js}^{exp} and modeled N_{js}^{mod} with the equation 16.

4.2. Effect of the impeller geometry on N_{js}

First, the off-bottom impeller clearance C was raised to the power of $1/3$ which was in accordance with literature data, stating that N_{js} become lower as the C/T ratio was reduced [17, 26]. In this study, the lowest value of C/T was 0.25, so it was admitted that flow patterns respected a 'double-eight' regime in the case of radial impellers. There was no pattern modification with the decrease of C/T [39, 40, 41].

Concerning the effect of the impeller diameter, it was found that N_{js} was proportional to D^{-1}, with the three models (Eqs. (14) to (16)). This trend was also in accordance with the literature [16, 17, 18]. A larger impeller presents a higher surface in contact with the continuous phase, and thus delivers a higher discharge stream, which facilitates the solids suspension. Moreover, our results showed that the impact of D/T ratio was much more significant than that of C/T, which is in agreement with previous works [18]. However, the -1 coefficient identified in our work was significantly lower than the one proposed by Nienow *et al.* [17], with a value of -2.21, or the -3.45 estimated by Arvinth *et al.* [18].

The last geometrical parameter considered in the models was the impeller shape, independently of its size. Depending on this shape, different model parameters were then determined for the constant K and the exponent a of particle volume fraction α_S to improve model precision. This choice was justified by the macroscopic structures of flow, promoting particle suspension either by particle aspiration or particle down-pushing according to the impeller design. In order to compare the different impellers used, both α_S and K effects on N_{js} were taken into account, and the $K.\alpha_S^a$ product was calculated for each impeller design. Products values are given in Table 6.

Table 6: Impact of the impeller design on N_{js} and classification.

Impeller design	$K.\alpha_S^a$		
	α_S=4 %	α_S=8 %	α_S=12 %
HTPGD	8.1	6.3	5.4
RT	5.0	3.9	3.3
EED	5.9	4.7	4.0
HTPGU	4.3	3.7	3.3
EEU	3.3	2.6	2.6

These values showed that the radial Rushton turbine and the impellers operating in mixed-flow regime displayed lower values, reflecting that it required less energy to lift particles by pushing them inward and aspirating them through the impeller direction than pushing them outward and making them slide along the wall, as it was represented in Fig. 4. Impellers could thus be classified, according to their efficiency to minimize N_{js}: the Elephant Ear impeller displayed lower N_{js} than the other impeller, especially at high solid concentrations and in up-pumping mode, whereas the HTPG impeller in down-pumping mode presented the highest value for N_{js}. But for cell culture applications, the impeller design has to be carefully chosen as displaying a lower N_{js} does not necessarily imply a minimization of hydromechanical stress induced. It was indeed shown by Collignon *et al.* that the Elephant impeller Ear displayed a lower N_{js}, but also higher Energy Dissipation / Circulation function than the Rushton turbine and the Marine propellers at the same power input indicating a higher exposition frequency of microcarriers to mechanical stresses with the Elephant Ear impeller [32]. For the investigation of an optimal impeller design, a parameter involving frequency exposure to hydromechanical stress should thus be taken into account, in addition to the N_{js} minimization.

4.3. Effect of the microcarrier concentration on N_{js}

As it was previously described and confirmed by the CFD, the particle concentration term was found to be a function of the impeller design in the $\alpha_S^{a_3}$ term, where a_3 displayed at least three values according to the agitation mode. An increase of N_{js} was observed with the solid volume fraction. The exponents obtained after the model resolution were close to the one proposed in the Zwietering correlation, where the solid mass fraction was raised to 0.13 (Eq. (1)). For microcarrier density, it corresponded to a solid volume fraction raised to 0.12. In the present study, the three values proposed by the new model were 0.07, 0.1 and 0.2, leading to a mean value of 0.12. The new model was thus broadly in accordance with the Zwietering correlation, but provided more precision with distinct values for each agitation mode.

4.4. Effect of microcarrier properties

Regarding only the particle diameter d_p effect on N_{js}, a negative value of -0.4 was found, which was in contradiction with correlations in the literature, presenting positive values [16, 17, 18]. In the present study, a dimensionless quantity, proportional to the number of particles was proposed instead of the d_p/D ratio, and was found to be raised to a positive value of 0.4/3. Hence, for a given particle concentration, larger beads led to lower number of particles, and thus to lower total interface area between the liquid and solid phases. For the case of microcarrier, more input power was required to suspend or avoid settling of a higher number of particles, despite their smaller diameter. Concerning particle density, it was involved through an Archimede number with a length scale characterizing the microcarrier cloud. As expected, denser particles required more input power, and thus a higher agitation rate to be fully suspended.

4.5. Comparison with the Zwietering correlation

In order to compare this new model (Eq. 16) with the Zwietering correlation, the S coefficient of the Eq. (1) has to be determined for each geometrical configuration of the study. To do that, experimental Zwietering coefficients S_{exp} were calculated from the experimental N_{js} measurements. The objective was then to gather all configurations varying the particle concentration or the microcarriers used, but displaying the same geometrical configuration, and determine a common S value. Because of the dispersed operating conditions, the majority of geometrical configurations had only one or two points. So, based on the results of this work, it was assumed that $N_{js} \propto C^{1/3}$, permitting to divide all measurements in 15 groups according to their common D/T value and impeller design. The ratio N_{js} was then expressed in function of the modified Zwietering function $f_{Zwietering,\ m}$ presented in Eqs. (17) and (18), inspired from a modified Zwietering correlation with $C^{1/3}$ extracted from the S coefficient (Eq. (17)). This $f_{Zwietering,\ m}$ term should be linear to N_{js}, with a slope corresponding to the common S_{calc} value of a given group. The S_{calc} values obtained after linear regressions are presented in Table 7.

$$N_{js,\ Zwietering\ calc} = S_{calc} . f_{Zwietering,\ m} \tag{17}$$

$$f_{Zwietering,\ m} = \nu_L^{0.1} . \left(\frac{g.(\rho_p - \rho_L)}{\rho_L} \right)^{0.45} .X^{\,0.13}.d_p^{\,0.2}.D^{\,-0.85}.C^{\,1/3} \tag{18}$$

Table 7: Adapted Zwietering coefficients S_{calc} values according to the impeller design and the D/T ratio.

	D/T		
Design	0.33	0.4	0.5
EED	7.1	7.1	6.3
HTPGD	11.8	11.3	11.1
RT	7.6	7.4	8.4
EEU	5.2	4.6	4.4
HTPGU	7.5	6.0	5.3

A comparison of this modified Zwietering model (Eq. (17)) with the new model (Eq. (16)) was finally performed and is represented in Fig. 7 The new model led to a relative error of 8.8 % with 96 % of points under 20 % deviation, whereas the adapted Zwietering model provided a relative error of 12.9 %, with 18 % of the absolute deviations over 20 % and leading up to 69 % deviation. The new model proposed thus better N_{js} prediction. Moreover, contrary to the Zwietering correlation, the constant K of the new model was only dependent of the impeller design. As animal cell cultures use media with water-like viscosities, no significant viscosity changes were considered in this model. Thus, higher model deviations may be expected for higher viscosity liquids.

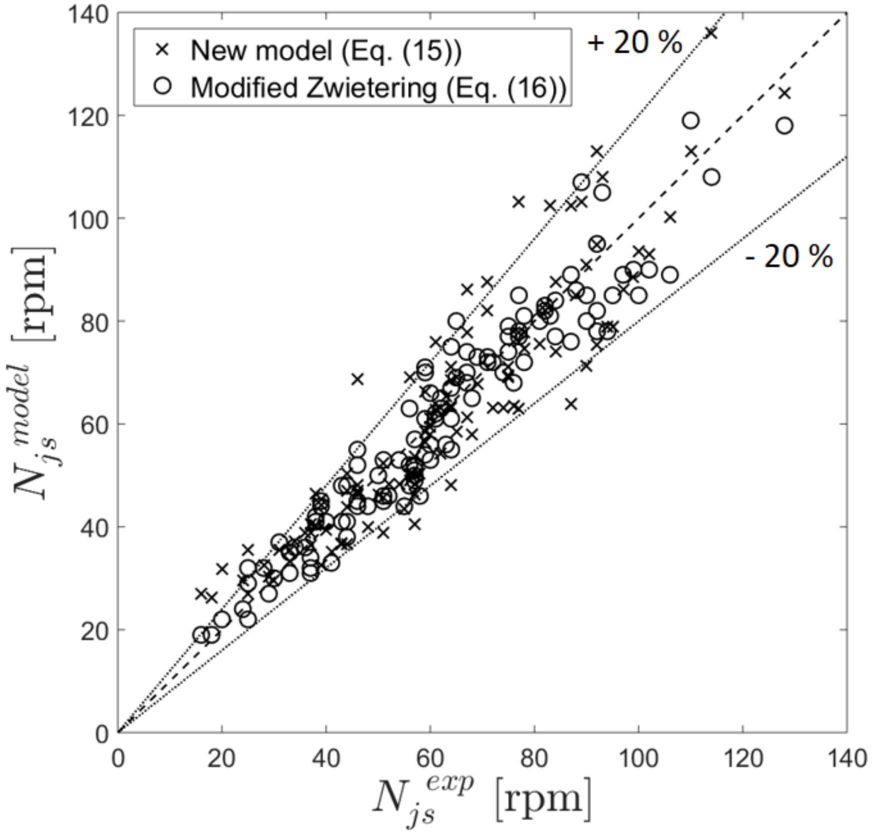

Figure 7: Comparison of modeled N_{js} and numerically adapted $N_{js,Zwietering}$

4.6. CFD-based method to predict N_{js}

Preliminary simulations were run to determine a suitable criterion to predict N_{js}. To do that, both PF and SF criteria (Eq. (11) and (12)) were calculated on the 200 mL minibioreactor geometry with 4 different impeller designs (EEU, EED, RT and Marine propeller in up-pumping mode). At the just-suspended state, the Reynolds numbers were comprised between 1 000 and 1 800, traducing a transitional regime. At the just-suspended state, using a standard-wall function for the near-wall turbulence modelling, values of y^+ below 15 were obtained which was not in the recommended validity range ($y^+ > 15$). Thus, the k-ϵ Scalable Wall Function was instead used. Simulations run at the experimental critical agitation rate N_{js}^{exp} provided SF values comprised between 0.08 % and 0.13 % and null values for PF. The SF criterion was thus used for the study with a critical value $SF^{\,crit}$ fixed at 0.10 %. Predicted critical agitation rates N_{js}^{simul} were then determined by looking for the agitation rate presented $SF = SF^{\,crit}$. Results are presented in Fig. 8 and led to a relative error of 9 %. This choice of criterion differed from the one of Tamburini *et al.* [22]. For glass bead suspensions, they found that a solid volume fraction based criterion presented better results than a one based on particle velocity. This second criterion was developed assuming that only particles presenting velocities equal to zero were considered to be unsuspended, unlike the SF criterion of the present study, in which particles with a very low residence time were considered to be unsuspended. This was in accordance with microcarriers suspension observations. Probably due to a density close to the liquid phase, the last particles to be suspended, as defined by the Zwietering criterion, were not totally motionless when staying in the bottom of the reactor.

The CFD-based method to predict N_{js} was then applied on 20 operating conditions of the 1.12 L reactor described in the experimental approach part. The k-ε model adaptation was not necessary for this reactor scale, displaying higher Reynolds number values of about 5 000, and so the Standard Wall Function was used. This system may be still considered in transitional regime, but the Standard Wall Function appeared to correctly solve the turbulent equations. As previously, $SF^{\,crit}$ value was firstly determined from SF values obtained from simulations run at the experimental critical agitation rate N_{js}^{exp}. In this case, $SF^{\,crit}$ was found at 0.20 %. This percentage indicated a quasi-motionless microcarrier volume of around 0.2 cm^3, which seemed to be representative of the experimental observations. N_{js}^{simul} were finally determined according to $SF^{\,crit}$ and compared to their corresponding experimental data. Comparison of the experimental and the predicted critical agitation rates are presented in Fig. 8 and displayed a mean relative error of 9 %. Higher deviations were observed with configurations presenting the lowest Reynolds number values, less than 2 100, at which the chosen turbulent models seemed to be inadequate. By removing these configurations, a lower mean relative error of 9 % was obtained in this restricted domain.

5. Conclusion

A new empirical correlation was established to predict N_{js} for microcarriers and was found to provide a better accuracy than the most commonly used Zwietering correlation. Another advantage displayed by the new model concerned the constant of the correlation. The traditional Zwietering correlation proposed a constant S function of the impeller design and both D/T and C/T ratios, which may be difficult to find in the literature. In the present study, the constants K were only dependent of the impeller design.

A dimensional analysis provided two other remarkable information. First, the influence of the particle volume fraction α_S seemed to be a function of the regime applied by the impeller. The determination of the constants K permitted to classify impellers, showing that the up-pumping mode led

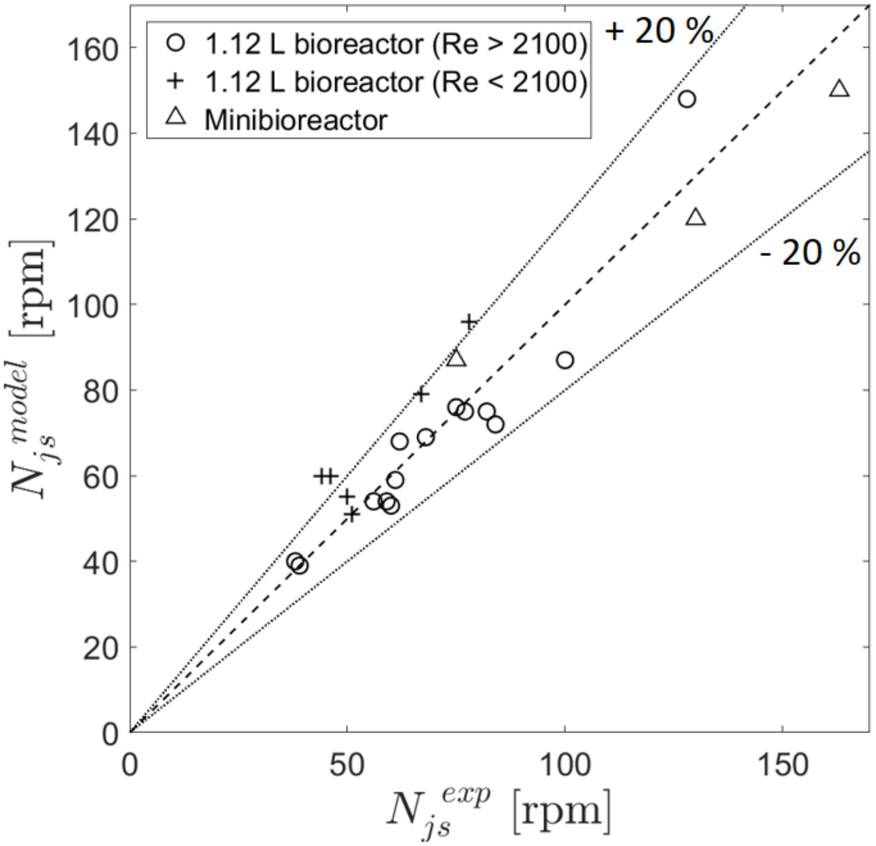

Figure 8: Comparison of experimental N_{js} and modeled N_{js} with the CFD-based method.

to lower N_{js} values. Secondly, in the case of microcarriers, the number of particles was found to better suit than the d_p/D ratio.

Finally, a CFD-based method was developed to numerically predict N_{js}. The models chosen and the method were validated according to two different working volumes, with 17 configurations for the specific vessel of this study. The particle residence time in the bottom was found to be the best criterion for microcarriers, with a critical value fixed at SF^{crit} of 0.20 %.

6. Acknowledgments

The authors would like to thank the French Agence Nationale de la Recherche (ANR) and the Interreg VA Grande Région program for their financial support. They also acknowledge Fabrice Blanchard (LRGP, Nancy) and Thierry Salmon (PEPs, Liège) for their technical contribution to this work.

Nomenclature

Variables

N	Impeller agitation rate	(s^{-1})
S	Zwietering coefficient (Eq. (1))	(-)
g	Gravity constant	(m s^{-2})
X	Mass concentration of particles	(%)
d	Diameter	(m)
D	Impeller diameter	(m)
C	Off-bottom clearance	(m)
T	Tank diameter	(m)
H	Tank height	(m)
V	Working volume	(m^3)
P	Global power input	(W)
$K_{1,2,3}$	Model impeller constants	(-)
$a_{1,2,3}$	Model constants	(-)
$b_{1,2,3}$	Model constants	(-)
$c_{1,2,3}$	Model constants	(-)
$d_{1,2,3}$	Model constants	(-)
PF	Packed fraction criterion (Eq. 11)	(-)
SF	Still fraction criterion (Eq. 12)	(-)
n_{exp}	Number of experiments	(-)

Greek letters

α	Volume fraction	(-)
μ	Dynamic viscosity	(Pa s)
ω	Optimization criterion (-)	

ν	Kinematic viscosity	(m^2 s^{-1})
ρ	Density	(kg m^{-3})
τ	Residence time	(s)

Dimensionless number

Ar	Archimede number	(-)
Re	Reynolds number	(-)
Fr	Froude number	(-)
Np	Newton number	(-)

Subscripts

js	Just-suspended state
up	Determination by N increase
down	Determination by N decrease
L	Liquid phase
m	Mixture
p	Particle
S	Solid phase
50	Median
5-95	Confidence interval
mean	Mean
mod	Modeled
exp	Experimental
crit	critical

References

[1] A. Stolzing, E. Jones, D. McGonagle, A. Scutt, Age-related changes in human bone marrow-derived mesenchymal stem cells: Consequences for cell therapies, Mechanisms of Ageing and Development 129 (2008) 163–173.

[2] J. Rowley, E. Abraham, A. Campbell, H. Brandwein, S. Oh, Meeting lot-size challenges of manufacturing adherent cells for therapy, BioProcess International 10 (2012) 7.

[3] A. L. Van Wezel, Growth of Cell-strains and Primary Cells on Micro-carriers in Homogeneous Culture, Nature 216 (1967) 64–65.

[4] A. S. Simaria, S. Hassan, H. Varadaraju, J. Rowley, K. Warren, P. Vanek, S. S. Farid, Allogeneic cell therapy bioprocess economics and optimization: Single-use cell expansion technologies, Biotechnology and Bioengineering 111 (2014) 69–83.

[5] T. Ma, A.-C. Tsai, Y. Liu, Biomanufacturing of human mesenchymal stem cells in cell therapy: Influence of microenvironment on scalable expansion in bioreactors, Biochemical Engineering Journal 108 (2016) 44–50.

[6] Q. A. Rafiq, K. M. Brosnan, K. Coopman, A. W. Nienow, C. J. Hewitt, Culture of human mesenchymal stem cells on microcarriers in a 5 l stirred-tank bioreactor, Biotechnology Letters 35 (2013) 1233–1245.

[7] T. Lawson, D. E. Kehoe, A. C. Schnitzler, P. J. Rapiejko, K. A. Der, K. Philbrick, S. Punreddy, S. Rigby, R. Smith, Q. Feng, J. R. Murrell,

M. S. Rook, Process development for expansion of human mesenchymal stromal cells in a 50 L single-use stirred tank bioreactor, Biochemical Engineering Journal 120 (2017) 49–62.

[8] C. Ferrari, F. Balandras, E. Guedon, E. Olmos, I. Chevalot, A. Marc, Limiting cell aggregation during mesenchymal stem cell expansion on microcarriers, Biotechnology Progress 28 (2012) 780–787.

[9] M. S. Croughan, J.-F. Hamel, D. I. C. Wang, Hydrodynamic effects on animal cells grown in microcarrier cultures, Biotechnology and Bioengineering 29 (1987) 130–141.

[10] T. M. Maul, D. W. Chew, A. Nieponice, D. A. Vorp, Mechanical stimuli differentially control stem cell behavior: morphology, proliferation, and differentiation, Biomechanics and Modeling in Mechanobiology 10 (2011) 939–953.

[11] T. R. Heathman, A. W. Nienow, Q. A. Rafiq, K. Coopman, B. Kara, C. J. Hewitt, Agitation and aeration of stirred-bioreactors for the microcarrier culture of human mesenchymal stem cells and potential implications for large-scale bioprocess development, Biochemical Engineering Journal 136 (2018) 9–17.

[12] C. J. Hewitt, K. Lee, A. W. Nienow, R. J. Thomas, M. Smith, C. R. Thomas, Expansion of human mesenchymal stem cells on microcarriers, Biotechnology letters 33 (2011) 2325–2335.

[13] R. S. Cherry, E. T. Papoutsakis, Physical mechanisms of cell damage in

microcarrier cell culture bioreactors, Biotechnology and Bioengineering 32 (1988) 1001–1014.

[14] A. C. Schnitzler, A. Verma, D. E. Kehoe, D. Jing, J. R. Murrell, K. A. Der, M. Aysola, P. J. Rapiejko, S. Punreddy, M. S. Rook, Bioprocessing of human mesenchymal stem/stromal cells for therapeutic use: Current technologies and challenges, Biochemical Engineering Journal 108 (2016) 3–13.

[15] A. Tamburini, A. Brucato, A. Cipollina, G. Micale, M. Ciofalo, CFD predictions predictions of sufficient suspension conditions in solid-liquid agitated tanks, International Journal of Nonlinear Sciences and Numerical Simulation 13 (2012) 427–443.

[16] T. N. Zwietering, Suspending of solid particles in liquid by agitators, Chemical Engineering Science 8 (1958) 244–253.

[17] A. Nienow, Suspension of solid particles in turbine agitated baffled vessels, Chemical Engineering Science 23 (1968) 1453–1459.

[18] S. Arvinth, P. G. Rao, T. Murugesan, Critical impeller speed for solid suspension in turbine agitated contactors, Bioprocess and Biosystems Engineering 14 (1996) 97–99.

[19] M. Kraume, Mixing times in stirred suspensions, Chemical Engineering & Technology 15 (1992) 313–318.

[20] A. Delafosse, C. Loubière, S. Calvo, D. Toye, E. Olmos, Solid-liquid suspension of microcarriers in stirred tank bioreactor-experimental and numerical analysis, Chemical Engineering Science 180 (2018) 52–63.

[21] K. Raghava Rao, V. Rewatkar, J. Joshi, Critical impeller speed for solid suspension in mechanically agitated contactors, AIChE Journal 34 (1988) 1332–1340.

[22] A. Tamburini, A. Cipollina, G. Micale, A. Brucato, M. Ciofalo, CFD simulations of dense solid–liquid suspensions in baffled stirred tanks: Prediction of suspension curves, Chemical Engineering Journal 178 (2011) 324–341.

[23] N. Kee, R. B. Tan, CFD simulation of solids suspension in mixing vessels, The Canadian Journal of Chemical Engineering 80 (2002) 1–6.

[24] A. Mersmann, F. Werner, S. Maurer, K. Bartosch, Theoretical prediction of the minimum stirrer speed in mechanically agitated suspensions, Chemical Engineering and Processing: Process Intensification 37 (1998) 503–510.

[25] K. Wichterle, Conditions for suspension of solids in agitated vessels, Chemical Engineering Science 43 (1988) 467–471.

[26] G. Baldi, R. Conti, E. Alaria, Complete suspension of particles in mechanically agitated vessels, Chemical Engineering Science 33 (1978) 21–25.

[27] S. Ibrahim, A. W. Nienow, Suspension of Microcarriers for Cell Culture with Axial Flow Impellers, Chemical Engineering Research and Design 82 (2004) 1082–1088.

[28] P. M. Armenante, E. U. Nagamine, Effect of low off-bottom impeller clearance on the minimum agitation speed for complete suspension of

solids in stirred tanks, Chemical Engineering Science 53 (1998) 1757–1775.

[29] M. Chudacek, Solids suspension behaviour in profiled bottom and flat bottom mixing tanks, Chemical Engineering Science 40 (1985) 385–392.

[30] M. S. Croughan, J.-F. P. Hamel, D. I. C. Wang, Effects of microcarrier concentration in animal cell culture, Biotechnology and Bioengineering 32 (1988) 975–982.

[31] Q. A. Rafiq, K. Coopman, A. W. Nienow, C. J. Hewitt, Systematic microcarrier screening and agitated culture conditions improves human mesenchymal stem cell yield in bioreactors, Biotechnology journal 11 (2016) 473–486.

[32] M.-L. Collignon, A. Delafosse, S. Calvo, C. Martin, A. Marc, D. Toye, E. Olmos, Large-Eddy Simulations of microcarrier exposure to potentially damaging eddies inside mini-bioreactors, Biochemical Engineering Journal 108 (2016) 30–43.

[33] E. Olmos, K. Loubiere, C. Martin, G. Delaplace, A. Marc, Critical agitation for microcarrier suspension in orbital shaken bioreactors: experimental study and dimensional analysis, Chemical Engineering Science 122 (2015) 545–554.

[34] M.-L. Collignon, A. Delafosse, M. Crine, D. Toye, Axial impeller selection for anchorage dependent animal cell culture in stirred bioreactors: methodology based on the impeller comparison at just-suspended speed of rotation, Chemical Engineering Science 65 (2010) 5929–5941.

[35] S. Kaiser, V. Jossen, C. Schirmaier, D. Eibl, S. Brill, C. van den Bos, R. Eibl, Fluid flow and cell proliferation of mesenchymal adipose-derived stem cells in small-scale, stirred, single-use bioreactors, Chemie Ingenieur Technik 85 (2013) 95–102.

[36] C. Schirmaier, V. Jossen, S. C. Kaiser, F. Jüngerkes, S. Brill, A. Safavi-Nab, A. Siehoff, C. Bos, D. Eibl, R. Eibl, Scale-up of adipose tissue-derived mesenchymal stem cell production in stirred single-use bioreactors under low-serum conditions, Engineering in Life Sciences 14 (2014) 292–303.

[37] V. Jossen, S. C. Kaiser, C. Schirmaier, J. Herrmann, A. Tappe, D. Eibl, A. Siehoff, C. van den Bos, R. Eibl, Modification and qualification of a stirred single-use bioreactor for the improved expansion of human mesenchymal stem cells at benchtop scale, Pharmaceutical Bioprocessing 2 (2014) 311–322.

[38] s. n. Fluent, Ansys fluent theory guide 15.0, Inc, Canonsburg, PA (2013).

[39] P. M. Armenante, E. U. Nagamine, Effect of low off-bottom impeller clearance on the minimum agitation speed for complete suspension of solids in stirred tanks, Chemical Engineering Science 53 (1998) 1757–1775.

[40] G. Montante, A. Brucato, K. Lee, M. Yianneskis, An experimental study of double-to-single-loop transition in stirred vessels, The Canadian Journal of Chemical Engineering 77 (1999) 649–659.

[41] G. Montante, K. Lee, A. Brucato, M. Yianneskis, Numerical simulations of the dependency of flow pattern on impeller clearance in stirred vessels, Chemical Engineering Science 56 (2001) 3751–3770.